Journal of Nuclear Materials 459 (2015) 37–43

Contents lists available at ScienceDirect

Journal of Nuclear Materials

journal homepage: www.elsevier.com/locate/jnucmat

Influence of instrument conditions on the evaporation behavior of uranium dioxide with UV laser-assisted atom probe tomography

B. Valderrama [a], H.B. Henderson [a], J. Gan [b], M.V. Manuel [a,*]

[a] Department of Materials Science and Engineering, University of Florida, Gainesville, FL 32611, USA
[b] Idaho National Laboratory, Idaho Falls, ID 83415, USA

HIGHLIGHTS

- Effect of temperature, laser energy, and detection rate on the evaporation of UO_2 was investigated.
- Laser energy can significantly affect the evaporation behavior of UO_2.
- Proper experimental conditions allows for an accurate investigation of UO_2 with APT.

ARTICLE INFO

Article history:
Received 19 July 2014
Accepted 29 December 2014
Available online 3 January 2015

ABSTRACT

Atom probe tomography (APT) provides the ability to detect subnanometer chemical variations spatially, with high accuracy. However, it is known that compositional accuracy can be affected by experimental conditions. A study of the effect of laser energy, specimen base temperature, and detection rate is performed on the evaporation behavior of uranium dioxide (UO_2). In laser-assisted mode, tip geometry and standing voltage also contribute to the evaporation behavior. In this investigation, it was determined that modifying the detection rate and temperature did not affect the evaporation behavior as significantly as laser energy. It was also determined that three laser evaporation regimes are present in UO_2. Very low laser energy produces a behavior similar to DC-field evaporation, moderate laser energy produces the desired laser-assisted field evaporation characteristic and high laser energy induces thermal effects, negatively altering the evaporation behavior. The need for UO_2 to be analyzed under moderate laser energies to produce accurate stoichiometry distinguishes it from other oxides. The following experimental conditions providing the best combination of mass resolving power, accurate stoichiometry, and uniform evaporation behavior: 50 K, 10 pJ laser energy, a detection rate of 0.003 atoms per pulse, and a 100 kHz repetition rate.

1. Introduction

With ever-increasing energy demands and concerns over nuclear waste, there is a need to push existing light water reactors (LWRs) to higher fuel burnups, while maintaining longer overall lifetimes [1]. These reactors primarily use enriched uranium dioxide (UO_2) as a fuel source [2], which undergoes a myriad of multiscale changes as nuclear fission progresses [3]. The presence of large thermal gradients and fission products leads to the formation of rim structures, stoichiometric variations, fission gas clustering, and multiphase precipitation [4–7]. Techniques such as X-ray photoelectron spectroscopy (XPS), scanning electron microscopy (SEM), and transmission electron microscopy (TEM) have made important contributions to the understanding of these processes, but there is a continuing need to detect early-stage nanoscale chemical variations in nuclear fuel more accurately and in three-dimensions. Furthermore, as more atom probe instruments that allow for the study of radioactive materials come online, the investigation of UO_2 using atom probe tomography will likely become increasingly common. Thus, fundamental run condition studies, as represented in this paper, can serve as an instrumental benchmark to the nuclear fuels community.

Uranium dioxide (UO_2), has been relatively unexplored by atom probe, owing to difficulties in preparation of radiological materials, has high technological and industrial relevance due to its pervasive use as a commercial nuclear fuel material [2]. UO_2 exhibits a fluorite crystal structure with an oxygen (O) to uranium (U) stoichiometry of 2.00 [2]. Its high dielectric constant, thermodynamic

* Corresponding author at: University of Florida, 152 Rhines Hall, Gainesville, FL 32611, USA. Tel.: +1 352 846 3780.
E-mail address: mmanuel@mse.ufl.edu (M.V. Manuel).

http://dx.doi.org/10.1016/j.jnucmat.2014.12.119
0022-3115/

stability, melting temperature, and reflectivity in the ultraviolet (UV) region make it attractive for numerous applications in nuclear, semiconductor, and optical industries [8,9].

Since its introduction, atom probe tomography (APT) has improved the length scale at which chemical variations can be measured. In this technique, a pulsed electric field or laser is used to extract surface ions from a sharp sample tip (<100 nm diameter), after which they are then accelerated toward a time-of-flight mass spectrometer with a position sensitive detector to determine the chemical identity of the ion and its original position [10–14]. Using this information, the sample tip is computationally reconstructed for in-depth analysis. A pulsed electric field is the primary method for extraction of surface ions for electrically conductive materials, but materials with poor electrical conductivity, such as oxides, require a pulsed laser to assist in the removal of surface ions by thermal excitation [15]. Although recent investigations have explored the physical mechanisms of evaporation, questions still remain regarding the sample and laser interactions and the mechanisms that assist in ion evaporation in oxides [16–21].

When studying poor electrical conductors, certain atom probe instrument parameters can lead to variations in compositional analysis caused by the preferential evaporation of specific ions or laser-induced heating artifacts leading to peak broadening and thermal peak tails in the mass spectrum [22–24]. Therefore, evaporation behavior must be optimized in order to obtain accurate chemistries from APT [15]. This paper presents a systematic study on the effect of sample temperature, detection rate, and laser energy on the chemical response of UO_2 in order to avoid the presence of artifact-induced inhomogeneities.

2. Materials and methods

For this investigation, single crystal depleted-UO_2 was chosen to avoid any changes in the evaporation behavior caused by grain boundaries and to produce samples with consistent crystal orientation. The single crystal depleted-UO_2 was fabricated by heating fused depleted-UO_2 with hyperstoichiometric UO_2 to 1900 K in hydrogen. Neutron diffraction measurements determined the single crystal had a crystalline fluorite structure, indicating its O:U ratio was 2.00 ± 0.001 [25]. Atom probe samples were fabricated by a focused ion beam (FIB) technique in which portions of UO_2 were attached to a prefabricated silicon micropost array and sharpened to a final tip diameter of approximately 70 nm [26]. To avoid a significant change in the electric field, only specimens of similar shank angles were compared in this study, with a standard deviation between specimens of 1.6°. The FIB used was an FEI 3D Quanta FEG and the local electrode atom probe was a CAMECA LEAP 4000X HR equipped with a 355 nm UV laser, with a spot size of 0.5 μm at full-width-half maximum (FWHM) at the specimen surface and a pulse duration of <15 ps. Each experimental condition consisted of a new specimen with at least six million ions collected.

Analysis of UO_2 in voltage mode (i.e. with only a voltage pulse and no laser-assisted evaporation) was attempted but samples prematurely fractured and no data was obtained from these runs. Therefore, a study of the UV laser's interaction with UO_2 is of key importance to understand how UO_2 performs in APT. Recent literature has reported a correlation between the wavelength of the laser and the band gap of the material and a consequent effect on the evaporation characteristics [27–30]. For the laser to assist in evaporation, its photon energy must be greater to or equal to the band gap energy the material to obtain full absorbance of the laser energy. However, absorption of the laser has been shown to be further enhanced by localized surface defects of the specimen produced during the tip fabrication process and the addition of an electric field will further reduce the band gap [19,31,32]. In this case, the photon energy of this UV laser (3.5 eV) is greater than the band gap energy of UO_2 (2.1 eV at room temperature [33] and 2.01 eV at 0 K based density functional theory simulation [34]).

The UV laser uses thermal excitation to assist in the evaporation of ions, therefore the thermal behavior of UO_2 must be mentioned. While UO_2 has adequate electrical conductivity as a semiconductor material, its thermal conductivity near the cryogenic operation temperature of the atom probe is poor. If too low of a specimen base temperature is selected for materials with decreasing thermal conductivity at cryogenic temperatures, it can lead to issues such as pronounced peak tails, affecting the measured results [35]. For this reason the specimen base temperature investigated was kept to a minimum of 35 ± 5 K, since below 30 K, UO_2 exhibits an anti-ferromagnetic phase transition that dramatically reduces its thermal conductivity [36].

For this investigation, laser energy, detection rate, and base temperature were varied to determine the specific factor(s) that had the greatest effect on data quality and to determine the combination of parameters that would produce an optimal data set, specifically having a lack of any preferential evaporation artifacts, accurate stoichiometry, and high mass resolving power. Samples were investigated at 35 or 50 K to avoid issues with heat dissipation that would be present at temperatures lower than 30 K due to the phase transition in UO_2 and higher specimen temperatures can induce surface ion migration [11,37,38]. Uranium's high atomic mass requires a lower pulse repetition rate, since the time of flight window can be too small to measure large mass-to-charge ions [21]. A constant pulse repetition rate of 100 kHz was therefore selected for this investigation such that the mass spectrometer can accommodate ions with longer flight times within this window. In these experiments, only ions emitted between the voltage range of 2–6 kV, and from a tip radius range of 30–40 nm were used in the analysis. The primary detection rate for this investigation was 0.003 atoms/pulse to minimize the likelihood of fracture. Once other variables were explored, the detection rate was increased to 0.01 atoms/pulse to a favorable outcome. The specific variables investigated in this study are listed in Table 1. For reconstruction, CAMECA's Interactive Visualization and Analysis Software (IVAS) version 3.6.6 was used. Assignment of the peaks was kept constant between each sample where similar peaks between sample conditions were present and labeled as indicated in Fig. 4. The peaks were ranged such as to only include approximately the full-width-tenth-maximum (FWTM) of each peak. A secondary electron image of each specimen was taken after sharpening in order to reconstruct the specimen in IVAS using the tip profile option.

3. Results

The necessary use of a UV laser to assist ion evaporation has been shown to cause uneven heating across the specimen, leading to artifacts such as compositional gradients [39,40]. Proper experimental conditions for APT are therefore necessary to obtain accurate chemical information. This section will illustrate the role of instrument parameters, specifically laser energy, detection rate,

Table 1
Atom probe run parameters investigated (constant 100 kHz pulse rate).

Laser energy (pJ)	Detection rate (atoms/pulse)	
	0.003	0.01
5	50 K	–
10	50 K	–
50	35 K, 50 K	35 K, 50 K
100	35 K, 50 K	–
200	50 K	–
300	50 K	–

and specimen base temperature, on the evaporation behavior of UO_2. Differences in these parameters produced varying effects, such as preferential evaporation features affecting local stoichiometry, differences in detected ionic species, degradation of mass resolving power, and stoichiometric deviations from the expected O:U of 2.00.

3.1. Preferential evaporation

The most energetically favorable surface plane in UO_2 is the (1 1 1) surface [41], which is also the most favorable for ions to field evaporate and has a threefold symmetry perpendicular to the specimen direction (the (1 1 1) pole) [42]. The addition of crystallographic features to the reconstructed specimen is detrimental for chemical analysis as specific ion types are evaporated along these crystallographic lines, potentially altering locally, the observed chemistry. The inhomogeneity in local chemistry at these crystallographic lines can significantly affect any true chemistry change [38]. The intensity of this feature was influenced by laser energy, as can be seen in Fig. 1, where top-down 2-dimension (2D) density hit maps of the samples are ordered from lowest to highest laser energy. Fig. 2 presents the distribution of UO^{n+} type ions, which are concentrated in areas of low overall atomic density, specifically along the crystallographic features. Gault et al. [43] attributes the increase in intensity of this crystallographic feature with laser energy to a temperature increase, causing ions to migrate to positions of lower coordination. In addition, similar behavior has been observed when field evaporating tungsten, molybdenum, and tantalum at elevated temperatures in field ion microscopy [44]. Altering the specimen base temperature had a small effect on the crystallographic features for specific laser energies, as presented in Fig. 3, but decreasing the detection rate made the feature more pronounced.

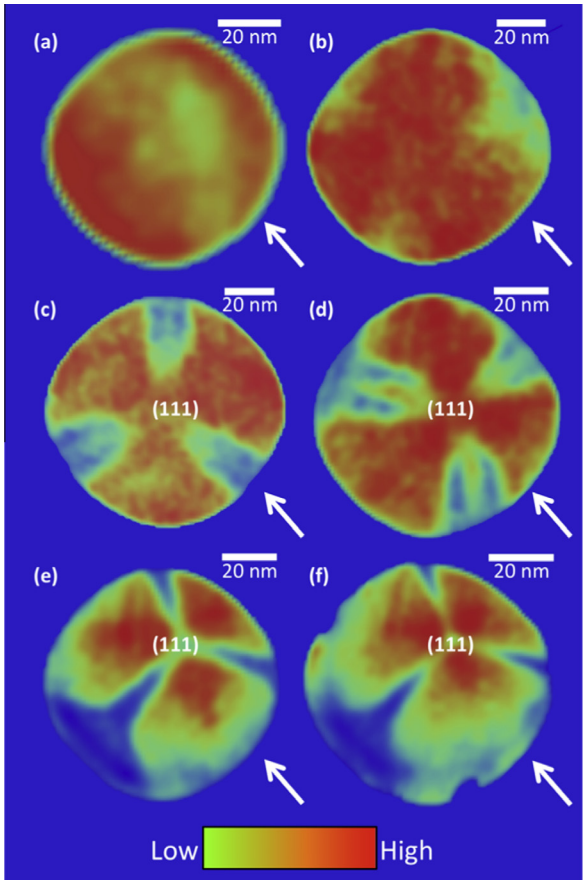

Fig. 1. 2-dimensional density hit maps of the UO_2 tips representing the influence of laser energy (a) 5 pJ, (b) 10 pJ, (c) 50 pJ, (d) 100 pJ, (e) 200 pJ, (f) 300 pJ on the preferential evaporation with constant 50 K, 100 kHz, 0.003 atoms/pulse. Arrows indicate the direction of the laser incidence. The bottom legend indicates number density of U^{n+}, O^{n+}, O_2^{n+}, UO^{n+}, and UO_3^{n+} ions.

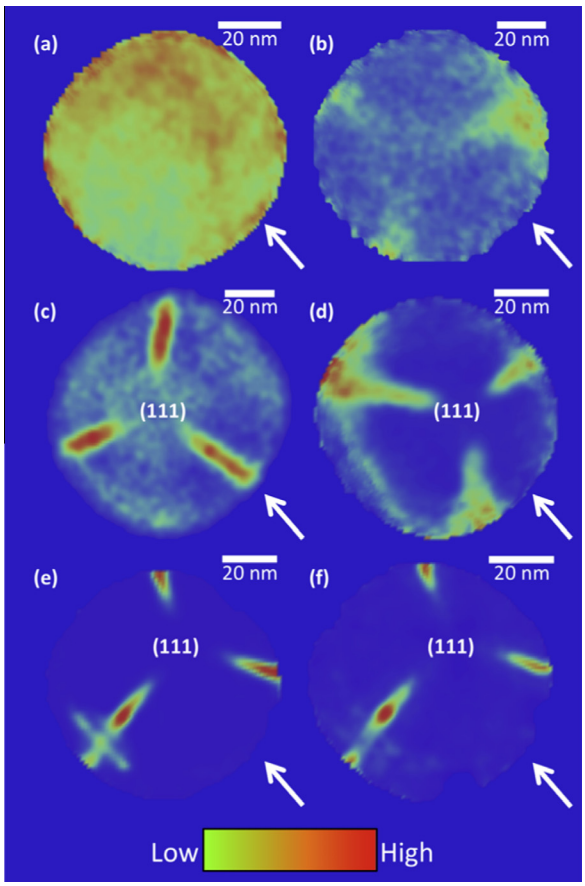

Fig. 2. Distribution of UO^{n+} type ions representing the influence of laser energy (a) 5 pJ, (b) 10 pJ, (c) 50 pJ, (d) 100 pJ, (e) 200 pJ, (f) 300 pJ on its appearance along the observed crystallographic features with constant 50 K, 100 kHz, 0.003 atoms/pulse. Arrows indicate the direction of the laser incidence.

Fig. 3 displays the effect of modifying detection rate and the laser pulse energy on induced density gradients at 35 and 50 K. Altering the base temperature produced the same results as illustrated in Fig. 1, while lowering detection rate made the density gradients more pronounced. In all of the images, the laser beam is incident on the sample on the lower right corner. Non-uniform evaporation originates due to the presence of the 3-fold crystallographic artifact at 10 pJ and is exacerbated with increasing laser energy.

3.2. Ion counts and types

The amount of a specific ion detected significantly influences the calculated stoichiometry, especially in oxides. For instance, Marquis et al. [45] has shown in the analysis of Al_2O_3, that the expected Al:O stoichiometry of 0.67 was not measured due to the majority of the ions detected being Al^{n+}, O^+, and O_2^+, providing an erroneous measured stoichiometry of 0.77 ± 0.3. For all samples in this investigation, the majority of the ions collected were UO_2^{n+} (n = 1, 2), followed by UO^{n+} (n = 1, 2). These ion types for UO_2 made its possible to calculate the stoichiometry very close to what is to be expected. A representative mass spectrum is shown in Fig. 4. U^{n+} ions counts were low for the run conditions investigated, as

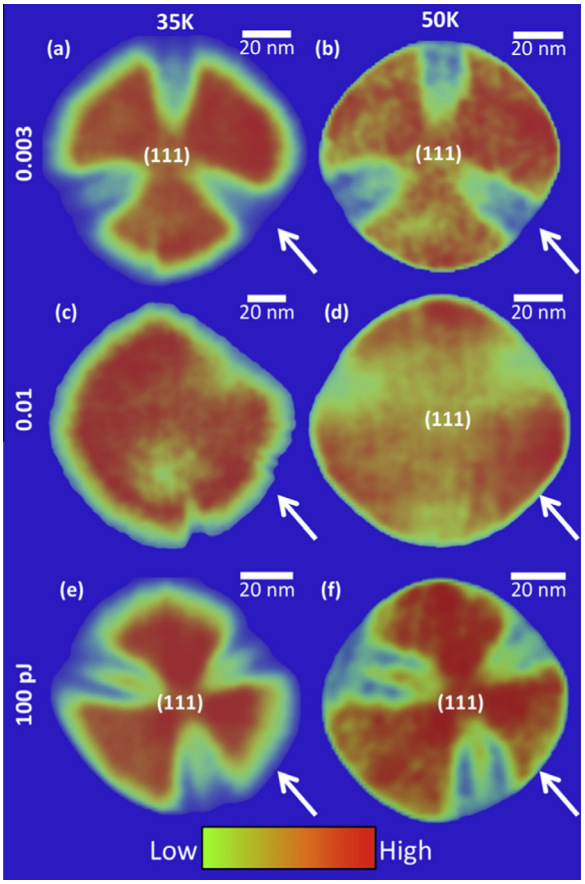

Fig. 3. Top-down view of the reconstructed UO_2 tips representing the influence of tip temperature for 50 pJ, 0.003 atoms/pulse, 100 kHz (a) 35 K, (b) 50 K; for 50 pJ, 0.01 atoms/pulse, 100 kHz (c) 35 K, (d) 50 K; and for 100 pJ, 0.003 atoms/pulse, 100 kHz (e) 35 K, (f) 50 K. The bottom legend indicates number density of U^{n+}, O^{n+}, O_2^{n+}, UO^{n+}, and UO_3^{n+} ions. Arrows indicate the direction of the laser incidence.

listed in Table 2. At higher laser energies above 100 pJ, the diversity of ions detected in atom probe decreased significantly with UO_2^{n+} ion types accounting for more than 97% of the ions detected.

3.3. Mass resolving power

Mass resolving power ($m/\Delta m$), where m is the mass-to-charge state ratio at the apex of a particular peak and Δm is the full-width

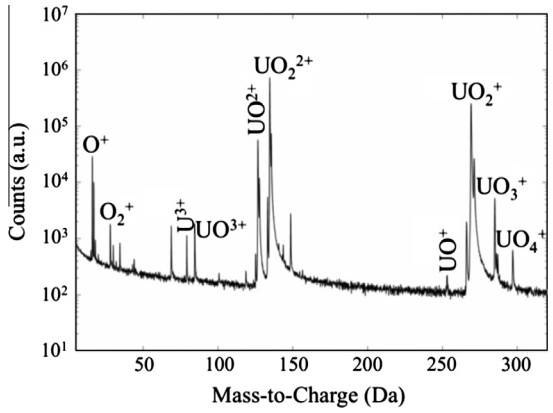

Fig. 4. Representative UO_2 mass spectrum for the following experimental conditions: 50 pJ, 100 kHz, 50 K, a detection rate of 0.003 atoms/pulse, and 60 million ions. The majority of ions detected are of the UO_2^{n+} type, followed by the UO^{n+} ion type.

Table 2
Influence of laser energy on the ion types detected. (Constants: 50 K, 100 kHz, detection rate of 0.003 atoms/pulse) Values in parenthesis indicate detection rate of 0.01 atoms/pulse. Superscript *n* indicates ion charge state of 1, 2, or 3.

Ion type	Ion distribution (%)					
	5 pJ	10 pJ	50 pJ	100 pJ	200 pJ	300 pJ
U^{n+}	3.93	0.03	0.05 (0.01)	0.02	0.00	0.00
O^{n+}	7.98	5.66	2.61 (1.01)	2.12	0.79	0.76
UO^{n+}	31.95	2.61	5.18 (2.69)	5.35	2.01	1.25
UO_2^{n+}	56.02	91.57	92.14 (95.25)	92.49	97.12	97.98
UO_3^{n+}	0.00	0.00	0.66 (1.01)	0.27	0.34	0.62

at a specific ratio of the peak maximum, is used to measure how well ion peaks can be differentiated from one another in a mass spectrum [15,46]. A greater mass resolving power enables more accurate peak identification because it reduces the chance of peak overlap, increasing chemical sensitivity. The mass resolving power was determined for the peak with the highest intensity, which was the UO_2^{2+} peak for all samples. Fitting a curve to this peak, the peak center and both the FWHM and FWTM were determined. These values for each run condition are listed in Table 3. In the range of sample conditions investigated, laser energy had the greatest influence on mass resolving power of UO_2, as presented in Fig. 5.

The effect of sample temperature and detection rate on mass resolving power and on the UO_2^{2+} peak is listed in Table 3. Generally, lower sample temperature decreased the mass resolving power and is presented in Fig. 5. Increasing the detection rate lowered mass resolving power. However, individual peaks in UO_2 do not overlap at the faster detection rate (0.01 compared to 0.003 atoms/pulse), indicating these faster detection rates can be used to reduce collection time without adverse effects, other than a higher likelihood of fracture due to a larger standing voltage.

3.4. Stoichiometry and multiple detector hits

It has previously been shown that instrument parameters can significantly influence evaporation behavior in APT analysis, leading to changes in measured stoichiometry [21]. Fig. 6 illustrates the changes in O:U ratio for the conditions investigated. These values were obtained from the bulk composition from the mass spectrum of each run condition, where all complex ions were decomposed into their constituents prior to the calculation. Results indicate that laser energy had a greater influence on stoichiometry than specimen base temperature and detection rate. Stoichiometry dependence on laser energy is illustrated graphically in Fig. 6.

Fig. 7 illustrates the amount of single ions hitting the detector for each condition under investigation. A high percentage of single detector hits is desired since the presence of multiple ions reaching the detector close, spatially or in time, can create ion pile-ups and make it difficult to discern chemical species. Changing the sample temperature and detection rate had little effect on the percentage of single detector hits. Laser energy, on the other hand, did affect this percentage.

Table 3
Mass resolving power, based on FWHM of the peak, for the sample conditions investigated in UO_2 as a function of laser energy, temperature and detection rate of a 0.003 atoms/pulse. Values in parenthesis indicate a detection rate 0.01 atoms/pulse. FWTM values are italized.

	5 pJ	10 pJ	50 pJ	100 pJ	200 pJ	300 pJ
35 K			725/*298* (*196*)	680/*315*		
50 K	366/*128*	825/*410*	897/*317* (*240*)	798/*372*	434/*177*	275/*117*

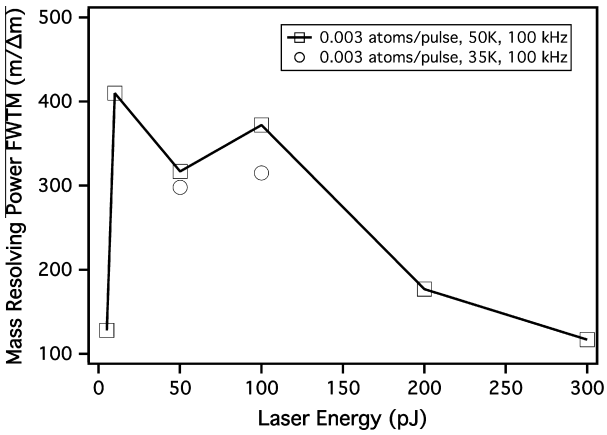

Fig. 5. Effect of laser energy on mass resolving power of the UO_2^{2+} peak (open squares) with the following conditions held constant: 50 K, detection rate of 0.003 atoms/pulse, and 100 kHz. Additional points on the effect of laser energy on mass resolving power of the UO_2^{2+} peak (open circles) with the following conditions held constant: 35 K, detection rate of 0.003 atoms/pulse, and 100 kHz.

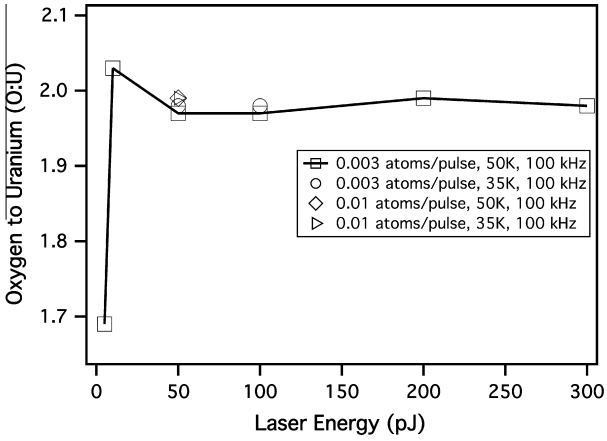

Fig. 6. Effect of laser energy on the oxygen-to-metal (O:U) ratio (open squares) with the following conditions held constant: 50 K, detection rate of 0.003 atoms/pulse, and 100 kHz. Additional points on the effect of laser energy on the oxygen-to-metal (O:U) ratio (open circles) with the following conditions held constant: 35 K, detection rate of 0.003 atoms/pulse, and 100 kHz. The effect of a detection rate of 0.01 atoms/pulse on O/U ratio at 50 K (open diamonds) and 35 K (open triangles), both with a constant 100 kHz repetition rate is also presented.

4. Discussion

4.1. Specimen temperature

Of the factors investigated, sample temperature had the least influence on the measured stoichiometry, only changing by 0.5% between 35 and 50 K. Modifying the detection rate changed the stoichiometry by 1% and laser energy changed it by 16%. These differences were measured by calculating the difference in calculated stoichiometry range for each of the factors investigated. However, the lower temperature was accompanied by a reduction in mass resolving power. This might be attributed to the phase transition point of UO_2 occurring at 30 K where the thermal conductivity is lower than at higher temperatures (1.2 W/(m K) at 35 K and 2.5 W/(m K) at 50 K [36]). Thus a lower mass resolving power could be due to delayed surface ion evaporation because of lower thermal conductivity, increasing the peak width [46]. A similar behavior was presented in $Fe_{1-x}O$, where too low of a specimen base temperature increases the thermal tail, decreasing the mass resolving power [35]. Thus, 50 K specimen base temperature is preferred for UO_2.

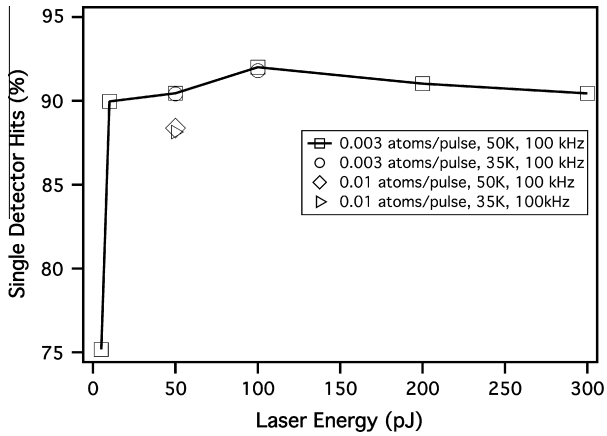

Fig. 7. Effect of laser energy on the percentage of single detector hits (open squares) with the following conditions held constant: 50 K, detection rate of 0.003 atoms/pulse, and 100 kHz. Additional points on the effect of laser energy the percentage of single detector hits (open circles) with the following conditions held constant: 35 K, detection rate of 0.003 atoms/pulse, and 100 kHz. The effect of a detection rate of 0.01 atoms/pulse on the percentage of single detector hits at 50 K (open diamonds) and 35 K (open triangles), both with a constant 100 kHz repetition rate is also presented.

4.2. Detection rate

Modifying the detection rate did not significantly affect the measured stoichiometry, as presented in Fig. 6, changing the O:U ratio by only 1%. It did change the ion distribution and mass resolving power as shown in Tables 2 and 3, respectively. Increasing the detection rate increases the applied standing voltage, which increases the applied electric field [15], typically promoting faster collection times. A potential drawback of a higher electric field is a decrease in the number of single ion hits, as seen in Fig. 7. Our results indicate, as presented in Fig. 6, that an increase in detection rate from 0.003 to 0.01 atoms/pulse leads to an increase in multiple detector hit events. It was observed that the mass resolving power ($m/\Delta m$) decreased for higher detection rate, but the stoichiometry was unaffected due to unconvoluted peak spacing and little peak overlap for pure UO_2. Thus higher detection rates may be used to reduce collection time for large data sets without significantly sacrificing the ability to calculate accurate stoichiometric ratios due to the absence of peak overlaps in UO_2. It was shown in this study that the detection rate did not alter stoichiometry, only causing a modest decrease in the percentage of single detector hit events and reduction in mass resolving power. Increasing the detection rate would produce a higher standing voltage and therefore increase the number of ions evaporating from the surface and can affect the evaporation behavior. However, the limited conductivity of UO_2 limits this increase due to specimen fracture at higher detection rates [15].

4.3. Laser energy

Understanding laser-specimen interactions are critical in laser-assisted APT. The UV laser of the APT instrument is strongly absorbed by UO_2, since the UV laser energy is larger than the band gap energy of UO_2. Uniform absorption of the laser is desired to avoid uneven evaporation [16]. For the 355 nm UV laser used in this study, the absorption coefficient (α) for UO_2 is expected to be $1.25 * 10^{-2}\,nm^{-1}$ [47]. This relates to a penetration depth (δ) of 80 nm, signifying that the near uniform absorption is expected

across the specimen [48]. The specifics of laser-specimen interaction in APT of oxide materials are not well understood in the literature, due to the highly complex nature of operant mechanisms. However, some trends in evaporation behavior based on input variables have been established. Li et al. [27] documented how the effect of laser energy may be divided into three different regimes. Low laser energies produce evaporation similar to direct current (DC) field evaporation, moderate laser energies produce the desired laser-assisted field evaporation, and large laser energies add unwanted thermal effects by increasing specimen temperature. Other studies in MgO [21] and CeO_2 [20] have shown that very low laser energies are ideal for accurate chemical analysis. The current investigation illustrates that laser energy strongly influenced mass resolving power, stoichiometry, and the evaporation behavior of UO_2.

The lowest laser energy condition investigated, 5 pJ, was accompanied by a larger percentage of UO^{n+}, U^{n+}, and O^{n+} ion types, as seen in Table 2, indicating the possible disassociation of the larger UO_2^{n+} complex ions. Under thermodynamic equilibrium, UO_2^+ is more stable than UO^+, with formation energies from bulk UO_2 of 114 kJ mol^{-1} and 606 kJ mol^{-1}, respectively and can be a reason why UO_2^{n+} type ions are preferred to evaporate [49]. However, it is important to note that the conditions of the atom probe instrument and tip geometry may be far from equilibrium conditions. At low laser energies, the standing voltage in APT must be higher to compensate for a lack of thermal excitation, causing higher electric fields and potential field ion dissociation. Field dissociation has been previously noted in APT of ceramic materials [20,50] at low laser energies. This may explain why individual U^{n+} and O^{n+} type ions accompany the increase in UO^{n+} type ions. This laser energy also exhibited poor mass resolving power (Fig. 5) a low number of single detector hits, as seen in Fig. 7. The poor mass resolving power at 5 pJ may be explained by the emission of ions being controlled by the standing DC electric field, as opposed the pulse laser, causing ions to emitted and detected with different flight times and therefore lead to peak broadening. Moreover, the measured O:U ratio of the 5 pJ sample (1.69) is much lower than for the other conditions, which were closer to the expected ratio of 2.00. This behavior at low laser energies indicates a different evaporation mechanism is active than at higher laser energies. If DC field evaporation is active, the applied voltage controls evaporation of the ions from the sample with minimal assistance from the laser due to its low energy [51]. Additionally, at a laser energy of 5 pJ, the background is higher than that for the higher laser energies investigated in work, as plotted in Fig. 8. A higher background can signify that while the DC field can cause ionization, specific ions cannot be correlated to time of flight data and thus are added to the background and seen as noise in the mass spectrum, thus providing further evidence that the DC field is contributing to the evaporation behavior of UO_2 at a laser energy of 5 pJ.

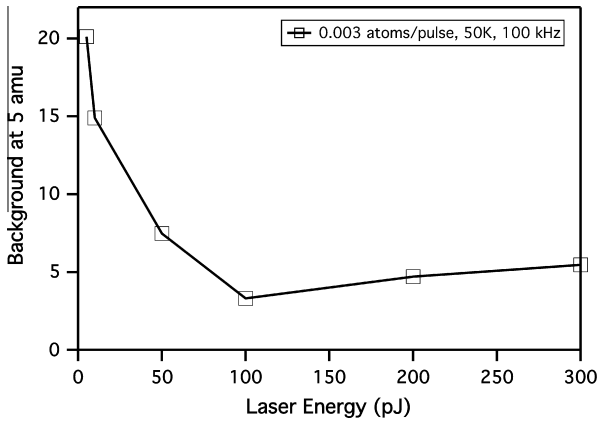

Fig. 8. Background of mass spectrum for UO_2 at a mass-to-charge state ratio of 5 amu.

For laser energies in the range of 10–100 pJ, mass resolving power is consistently optimal. The percentages of ions were also similar within this range, indicating that the mechanism of evaporation is stable over this range of laser energies. The stoichiometry in this range was close to the expected value of 2.00, with 10 pJ being the closest to this value. However, a crystallography-dependent preferential evaporation artifact was evident at laser energies greater than 50 pJ, seen in Fig. 1. Other than this artifact, this range produced satisfactory laser-assisted field evaporation in UO_2. The need of moderate laser energies to obtain accurate chemistries in UO_2 differs from other oxides, namely CeO_2 [20] and MgO [21], which require very low laser energies.

Higher laser energies can cause sample overheating, resulting in the evaporation of more complex ions and poorer mass resolving power. This effect is especially active in materials with poor thermal conductivity [40,46]. The use of high laser energies can lead to higher surface temperatures and with the limited ability of UO_2 to dissipate heat effectively, can cause a spread of the surface ions being evaporated, degrading mass resolving power [52]. This behavior was observed in UO_2 at laser energies of 200 pJ and above, shown in Fig. 3 and presented in Table 2. Higher laser also caused a decrease in ion type diversity, since greater than 97% of all ions detected were of the UO_2 type, since it is the most thermodynamically stable ion and adequate energy is available for it to be ionized.

5. Conclusions

In this study of APT run parameters on UO_2, it was found that evaporation and laser conditions can affect chemical analysis. The influence of sample temperature, detection rate, and laser pulse energy on the stoichiometry, mass resolving power, ion-type dependent evaporation, and localized in-homogeneities on single crystal depleted-UO_2 for a CAMECA LEAP 4000X HR instrument equipped with a UV-laser was presented. Our results indicated that the following run conditions: 10 pJ laser energy, a detection rate of 0.003 atoms/pulse, 50 K specimen base temperature, and 100 kHz repetition rate were the ideal setting for UO_2 since it provided the greatest variety in ion-types detected, high mass resolving power, near expected O:U ratio, composition uniformity, and avoided any crystallographic dependent evaporation artifact. Additionally, across the spectrum of laser energies, three different evaporation behaviors were apparent. At 5 pJ or less, the O:U ratio was inaccurate, higher background levels were present in the mass spectrum and mass resolving power was poor due to a DC field evaporation mechanism. Moderate laser energies of 10–100 pJ produced an O:U ratio close to what is expected and high mass resolving power through laser-assisted field evaporation. Laser energies at 200 pJ and larger reproduced the O:U ratio accurately, but showed diminished mass resolving power because of thermal effects. Although in this work, laser energy is highlighted to be a principal contributor to the evaporation characteristics of UO_2, it is important to note that evaporation is largely dependent on the applied field, where laser energy acts as a co-contributor alongside the standing voltage and tip geometry [15]. However, UO_2's limited conductivity hinders the ability to alter the applied field by solely relying on changes in the detection rate or specimen geometry. Thus, laser energy can be used as the primary driver of evaporation behavior in UO_2.

Acknowledgments

This paper is based on the work supported as part of the Center for Materials Science of Nuclear Fuel, an Energy Frontier Research

Center funded by the U.S. Department of Energy, Office of Science, Office of Basic Energy Sciences under Award Number FWP 1356. Use of the FIB and atom probe instrumentation at the Center for Advanced Energy Studies was supported by the U.S. Department of Energy, Office of Nuclear Energy under DOE Idaho Operations Office Contract DE-AC07-051D14517. The authors would also like to thank Dr. William Buyers for providing the UO_2 sample used in this study and Dr. Yaqaio Wu for assistance in running the atom probe.

References

[1] Nuclear Energy Research and Development Roadmap, in: U.S. Department of Energy, 2010.
[2] D.R. Olander, Fundamental Aspects of the Performance of Nuclear Reactor Fuel Elements, Technical Information Center, Office of Public Affairs, Springfield, VA, 1976.
[3] V.V. Rondinella, T. Wiss, Mater. Today 13 (2010) 24–32.
[4] J. Bruno, R.C. Ewing, Elements 2 (2006) 343–349.
[5] L.E. Thomas, C.E. Beyer, L.A. Charlot, J. Nucl. Mater. 188 (1992) 80–89.
[6] F.C. Iglesias, B.J. Lewis, P.J. Reid, P. Elder, J. Nucl. Mater. 270 (1999) 21–38.
[7] S.M. Bruemmer, E.P. Simonen, P.M. Scott, P.L. Andresen, G.S. Was, J.L. Nelson, J. Nucl. Mater. 274 (1999) 299–314.
[8] J.K. Fink, J. Nucl. Mater. 279 (2000) 1–18.
[9] Q. Chen, X. Lai, T. Tang, B. Bai, M. Chu, Y. Zhang, S. Tan, J. Nucl. Mater. 401 (2010) 118–123.
[10] T.F. Kelly, M.K. Miller, Rev. Sci. Instrum. 78 (2007) 031101.
[11] A. Cerezo, P.H. Clifton, A. Gomberg, G.D.W. Smith, Ultramicroscopy 107 (2007) 720–725.
[12] E.W. Müller, J.A. Panitz, S.B. McLane, Rev. Sci. Instrum. 39 (1968) 83–86.
[13] D. Blavette, A. Bostel, J.M. Sarrau, B. Deconihout, A. Menand, Nature 363 (1993) 432–435.
[14] A. Cerezo, P.H. Clifton, M.J. Galtrey, C.J. Humphreys, T.F. Kelly, D.J. Larson, S. Lozano-Perez, E.A. Marquis, R.A. Oliver, G. Sha, K. Thompson, M. Zandbergen, R.L. Alvis, Mater. Today 10 (2007) 36–42.
[15] B. Gault, Atom Probe Microscopy, Springer, New York, 2012.
[16] A. Vella, B. Mazumder, G. Da Costa, B. Deconihout, J. Appl. Phys. 110 (2011) 044321.
[17] F. Vurpillot, J. Houard, A. Vella, B. Deconihout, J. Phys. D: Appl. Phys. 42 (2009) 125502.
[18] T.F. Kelly, A. Vella, J.H. Bunton, J. Houard, E.P. Silaeva, J. Bogdanowicz, W. Vandervorst, Curr. Opin. Solid State Mater. Sci. 18 (2014) 81–89.
[19] E.P. Silaeva, M. Karahka, H.J. Kreuzer, Curr. Opin. Solid State Mater. Sci. 17 (2013) 211–216.
[20] R. Kirchhofer, M.C. Teague, B.P. Gorman, J. Nucl. Mater. 436 (2013) 23–28.
[21] A. Devaraj, R. Colby, W.P. Hess, D.E. Perea, S. Thevuthasan, J. Phys. Chem. Lett. 4 (2013) 993–998.
[22] J. Houard, A. Vella, F. Vurpillot, B. Deconihout, Phys. Rev. B 81 (2010) 125411.
[23] L. Yao, J.M. Cairney, C. Zhu, S.P. Ringer, Ultramicroscopy 111 (2011) 648–651.
[24] M.K. Miller, G.D.W. Smith, J. Vac. Sci. Technol. 19 (1981) 57–62.
[25] J.W.L. Pang, W.J.L. Buyers, A. Chernatynskiy, M.D. Lumsden, B.C. Larson, S.R. Phillpot, Phys. Rev. Lett. 110 (2013) 157401.
[26] K. Thompson, D. Lawrence, D.J. Larson, J.D. Olson, T.F. Kelly, B. Gorman, Ultramicroscopy 107 (2007) 131–139.
[27] F. Li, T. Ohkubo, Y.M. Chen, M. Kodzuka, K. Hono, Ultramicroscopy 111 (2011) 589–594.
[28] O. Mountanabbir, D. Isheim, D.N. Seidman, Y. Kawamura, K.M. Itoh, Appl. Phys. Lett. 98 (2011).
[29] K. Hono, T. Ohkubo, Y.M. Chen, M. Kodzuka, K. Oh-ishi, H. Seperhi-Amin, F. Li, T. Kinno, S. Tomiya, Y. Kanitani, Ultramicroscopy 111 (2011) 576–583.
[30] B. Gault, Y.M. Chen, T. Moody, K. Ohkubo, K. Hono, J. Appl. Phys. 110 (2011) 094901.
[31] M. Tsukada, H. Tamura, K.P. McKenna, A.L. Shluger, Y.M. Chen, T. Ohkubo, K. Hono, Ultramicroscopy 111 (2011) 567–570.
[32] T.T. Tsong, Surf. Sci. 70 (1978) 211–233.
[33] J. Schoenes, J. Appl. Phys. 49 (1978) 1463–1465.
[34] B. Szpunar, J. Szpunar, J. Phys. Chem. Solids 74 (2013) 1632–1639.
[35] M. Bachhav, R. Danoix, F. Danoix, B. Hannoyer, S. Ogale, F. Vurpillot, Ultramicroscopy 111 (2011) 584–588.
[36] K. Aring, A.J. Sievers, J. Appl. Phys. 38 (1967) 1496–1498.
[37] B. Gault, F. Vurpillot, A. Bostel, A. Menand, B. Deconihout, Appl. Phys. Lett. 86 (2005) 094101.
[38] B. Gault, F. Danoix, K. Hoummada, D. Mangelinck, H. Leitner, Ultramicroscopy 113 (2012) 182–191.
[39] M. Muller, G.D.W. Smith, B. Gault, C.R.M. Grovenor, J. Appl. Phys. 111 (2012) 064908.
[40] G. Sha, A. Cerezo, G.D.W. Smith, Appl. Phys. Lett. 92 (2008) 043503.
[41] P.W. Tasker, Surf. Sci. 87 (1979) 315–324.
[42] B. Gault, M.P. Moody, J.M. Cairney, S.P. Ringer, Mater. Today 15 (2012) 378–386.
[43] B. Gault, A. La Fontaine, M.P. Moody, S.P. Ringer, E.A. Marquis, Ultramicroscopy 110 (2010) 1215–1222.
[44] S. Nakamura, T. Kuroda, Surf. Sci. 17 (1969) 346–358.
[45] E.A. Marquis, N.A. Yahya, D.J. Larson, M.K. Miller, R.I. Todd, Mater. Today 13 (2010) 34–36.
[46] J.H. Bunton, J.D. Olson, D.R. Lenz, T.F. Kelly, Microsc. Microanal. 13 (2007) 418–427.
[47] T.R. Griffiths, H.V.S.A. Hubbard, G.C. Allen, P.A. Tempest, J. Nucl. Mater. 151 (1988) 313–317.
[48] B. Valderrama, H.B. Henderson, L. He, J. Pakarinen, J. Gan, T. Allen, M.V. Manuel, Irradiation induced chemistry changes in oxide fuel materials, in: TMS Annual Meeting, San Diego, CA, 2014.
[49] J. Marçalo, J.K. Gibson, J. Phys. Chem. A 113 (2009) 12599–12606.
[50] M. Müller, D.W. Saxey, G.D.W. Smith, B. Gault, Ultramicroscopy 111 (2011) 487–492.
[51] G. Sha, S.P. Ringer, Ultramicroscopy 109 (2009) 580–584.
[52] F. Tang, B. Gault, S.P. Ringer, J.M. Cairney, Ultramicroscopy 110 (2010) 836–843.